

Smart Electrolytes for Lithium Batteries with Reversible Thermal Protection at High Temperatures

Qian Yu,^[a] Wei Sun,^[a] Shuai Wang,^[a, b] Qian Qiu,^[a] Wenjun Zhang,^{*[b]} Haoran Tian,^[a] Lan Xia,^{*[a, c]} and Peter Müller-Buschbaum^{*[c]}

Battery safety is a multifaceted concern, with thermal runaway standing out as a primary issue. In this work, we introduce a novel temperature-responsive, self-protection electrolyte governed by the phase separation dynamics of poly (butyl methacrylate) (PBMA) in lithium salt/tetraglyme (G4) blends. This innovation effectively mitigates the risks associated with thermal runaway in lithium batteries. Our electrolyte exhibits a temperature-responsive-recovery characteristic, imparting intelligent capabilities to lithium batteries. At temperatures of $>105^{\circ}\text{C}$, the electrolyte transitions from a homogeneous phase to a segregated state, comprising a PBMA-rich phase with low conductivity and a high conductivity phase containing dis-

solved lithium salt in G4. The deposition of the PBMA-rich phase on the electrode surface obstructs the ion transport, thereby averting a thermal runaway. Subsequently, upon returning to room temperature of 25°C , the electrolyte reverts to its homogeneous, highly conductive state, with battery capacity resuming at approximately 94%. Thus, our electrolyte offers a robust, reversible, smart self-protection for batteries. Additionally, it demonstrates exceptional cycling performance at room temperature. Our findings open new avenues for thermo-reversible and self-protective electrolytes, advancing the safe and widespread adoption of lithium-ion batteries.

1. Introduction

Currently, lithium-ion batteries (LIBs) stand at the forefront of energy storage technology owing to their remarkable attributes including high energy density, high operating voltage, no memory effect, prolonged cycle life, and eco-friendliness.^[1-3] Traditional LIB electrolytes typically comprise lithium hexafluorophosphate (LiPF_6) dissolved in carbonate-based solvents.^[4-6] However, LiPF_6 is known for its instability and adverse environmental impact. Notably, even slight moisture can trigger the release of highly toxic and corrosive HF, necessitating stringent dry room conditions during LIB manufacturing and thereby escalating production costs. Moreover, the instability of LiPF_6 complicates the battery recycling process, raising environ-

mental concerns.^[7-10] Furthermore, linear carbonates such as dimethyl carbonate (DMC) and ethyl methyl carbonate (EMC) exhibit high volatility and flammability,^[11-14] rendering LIBs susceptible to thermal abuse and subsequent safety hazards.^[15]

Battery safety is a multifaceted issue, with thermal runaway being the most pressing concern. Elevated temperatures trigger various detrimental side reactions, including the decomposition of the electrode protection layer ($60\text{--}110^{\circ}\text{C}$), anode-electrolyte reactions ($\sim 100^{\circ}\text{C}$), and separator melting ($120\text{--}150^{\circ}\text{C}$), exacerbating secondary reactions and culminating in uncontrollable thermal runaway, often resulting in smoking, fires, or even explosions. Ensuring battery safety necessitates the implementation of sensing-response measures to avert thermal runaway, particularly at critical temperatures around 110°C . In practical applications (fast charging, temperature influence, and other effects), batteries may suffer from multiple cases of potential thermal runaway, which calls for thermal-responsive self-protection strategies.^[16-19]

In recent years, numerous strategies have emerged to enhance the safety of LIBs (as detailed in Table S1), encompassing the utilization of heat insulation materials,^[20,21] positive temperature coefficient (PTC) materials,^[22,23] temperature-responsive separators,^[24] and temperature-sensitive electrolytes.^[25,26] For example, Ai et al. proposed a temperature-sensitive cathode with conductive poly(3-decyliophene) (P3DT), exhibiting an appropriate PTC effect.^[27] With a PTC transition temperature of $80\text{--}110^{\circ}\text{C}$, P3DT exhibits a sharp increase in resistance when the battery temperature surpasses 110°C , effectively closing the current transport and averting thermal runaway. Consequently, the material provides one-time thermal protection for $\text{Li} \parallel \text{LiCoO}_2$ batteries at 110°C while allowing for continued battery operation, maintaining a discharge capacity of 50 mAh g^{-1} at the critical temperature.

[a] Q. Yu,⁺ W. Sun,⁺ S. Wang, Q. Qiu, H. Tian, L. Xia

Faculty of Maritime and Transportation, Ningbo University, No. 169 Qixing South Road, Ningbo Meishan Free Trade Zone, Ningbo, Zhejiang 315832 P. R. China

E-mail: xialan@nbu.edu.cn

[b] S. Wang, W. Zhang

College of New Energy, Ningbo University of Technology, Ningbo, 315211, China

E-mail: zhangwj@nbu.edu.cn

[c] L. Xia, P. Müller-Buschbaum

Technical University of Munich, TUM School of Natural Sciences, Department of Physics, Chair for Functional Materials, James-Franck-Str. 1, 85748 Garching, Germany

E-mail: xialan@nbu.edu.cn

muellerb@ph.tum.de

 Supporting information for this article is available on the WWW under <https://doi.org/10.1002/batt.202400339>

 © 2024 The Authors. *Batteries & Supercaps* published by Wiley-VCH GmbH. This is an open access article under the terms of the Creative Commons Attribution License, which permits use, distribution and reproduction in any medium, provided the original work is properly cited.

Additionally, their team introduced a temperature-responsive microspheres-coated separator–ethylene-vinyl acetate copolymer (EVA) microspheres-coated separator.^[28] With a melting point of 90 °C, the EVA microspheres melt upon reaching this temperature, obstructing the micropores of the separator and halting Li⁺ transport between electrodes, resulting in a sharp decrease in discharge capacity to 0 mAh g⁻¹, effectively terminating Li||LiCoO₂ battery operation. This data underscores the excellent thermal self-protection capability of the thermal shutdown separator. However, both thermal self-protection strategies mentioned above, which operate by blocking electron/ion transport, offer one-time, disposable, and irreversible protection, rendering the batteries unusable once activated. Consequently, researchers are exploring alternative methods to provide thermal protection, emphasizing the importance of thermal-responsive reversibility for battery safety.

In our previous research, we unveiled a thermo-reversible and self-protective electrolyte characterized by lower critical solution temperature (LCST) phase separation behavior.^[29] This electrolyte comprised lithium bis(trifluoromethanesulfonyl)imide (LiTFSI) and poly(benzyl methacrylate) (PBMA) dissolved in 1-ethyl-3-methylimidazolium bis(trifluoromethanesulfonyl)imide ([EMIM][TFSI]). With an LCST of 110 °C, heating the electrolyte above this threshold triggered the separation into a low conductivity PBMA-rich phase and a high conductivity phase containing [EMIM][TFSI] and LiTFSI.^[30–34] The deposition of the PBMA-rich phase on the electrode surface suppressed ion transport, abruptly halting battery operation. Upon returning to room temperature, the electrolyte reverted to a homogeneous, highly conductive phase, with battery capacity resuming at approximately 95 %. Unfortunately, the high viscosity of the ionic liquid [EMIM][TFSI]^[35] impeded the electrolyte's room temperature cycling performance and rate capability. Additionally, the relatively high cost of [EMIM][TFSI] posed a barrier to widespread application. Therefore, there is a demand for thermal-responsive self-protection electrolytes with low viscosity and cost-effectiveness, offering better application prospects. Previous literature by Masayoshi et al. showcased a system composed of PBMA, LiTFSI, and tetraglyme (G4) exhibiting obvious LCST phase separation behavior.^[36] Moreover, G4 is widely used in the electrolytes of lithium-ion batteries, renowned for their excellent cycle stability.^[37–39] Considering the extensive proposals for polymer-based membranes in Li-ion batteries,^[40–42] the PBMA/LiTFSI-G4 system holds promise as a new thermo-reversible and self-protective electrolyte poised for broader application.

As compared in Table S1, all the previous strategies suffer from one or more limitations, and they cannot satisfy all the needs of thermal protection. In this study, we prepare a thermal-responsive, self-protective smart electrolyte utilizing phase separation behavior of PBMA in lithium salt/tetraglyme blends. Our thermal-responsive, smart electrolyte is not only low viscosity and low cost but also provides highly precise (~105 °C) and reversible protection, which represents a significant progress in the high-safety electrolyte. Utilizing this electrolyte in Li||LiFePO₄ batteries (at 5 wt% PBMA-0.5 M LiTFSI/G4), we achieve remarkable cycle stability, retaining

93.50 % of capacity and maintaining an average Coulombic efficiency of 99.86 % over 200 cycles. Upon reaching 105 °C, the battery's reversible capacity dramatically decreases to a mere 4 mAh g⁻¹, rendering it nearly inactive. However, upon cooling back to room temperature, the battery's capacity promptly resumes to 94 %, facilitated by the electrolyte returning to a homogeneous phase. This underscores the highly precise and reversible thermal protection afforded by the 5 wt% PBMA-0.5 M LiTFSI/G4 electrolyte. To our knowledge, such smart and self-protective electrolytes, exhibiting outstanding room-temperature cycling performance coupled with high-temperature shutdown characteristics have been previously reported. Our findings present novel avenues for exploring temperature-sensitive, smart electrolytes in future research endeavors.

2. Results and Discussion

2.1. Characterization and Optimization of the PBMA-LiTFSI/G4 Electrolytes

It is well known that the conductivity of electrolytes has a direct influence on the cycle life and performance of the battery.^[43] We measure the conductivity of different electrolytes, as shown in Figure 1a–b. First, in order to explore the influence of LiTFSI concentration, we set PBMA concentration to 5 wt% tentatively. The conductivity at room temperature is 0.39, 0.79, 1.86, and 2.42 mS cm⁻¹ for 0.1, 0.2, 0.5, and 0.8 mol L⁻¹ (M) LiTFSI, respectively. The conductivity of 0.1 and 0.2 M LiTFSI is lower than 1 mS cm⁻¹, it does not meet the requirements for conductivity of electrolytes. Although both 0.5 and 0.8 M LiTFSI have high ionic conductivity, 0.5 M LiTFSI exhibits the best room-temperature cycling performance (see Figure 2). Therefore, 0.5 M LiTFSI is an ideal choice. Thus, we fix the 0.5 M LiTFSI concentration and continue to explore the effect of the PBMA concentration. The room temperature conductivity is 1.97, 1.86 and 1.58 mS cm⁻¹ for the 2, 5, and 8 wt% PBMA, respectively (Figure 1b), showing a slight decrease with the increase of PBMA concentration. This finding indicates that PBMA has little influence on the ionic conductivity of the system.

In order to further investigate the system, Raman spectra are implemented, as shown in Figure 1c. Compared with the pure LiTFSI, the S–N peak at ~750 cm⁻¹ shifts to a lower wavenumber with the addition of PBMA and G4.^[44] It indicates that the oxygen-containing groups in either PBMA or G4 may interact with Li⁺, which weakens the Li⁺...TFSI⁻ interactions.^[45] The intensity of the vibration peak (~1000 cm⁻¹) of the mono-benzene ring increases with the increase of PBMA concentration. In addition, the peak at 1215 cm⁻¹ corresponds to the bending vibration of the PBMA framework. When the PBMA concentration increases to 5 wt%, the peak (1215 cm⁻¹) starts to appear, indicating that 5 wt% is a critical point compared with 2 wt% and 8 wt% PBMA. At the same time, we carry out linear sweep voltammetry (LSV) tests (Figure 1d). As the concentration of PBMA increases, the oxidation stability of these electrolytes slightly decreases. The oxidation potential of 5 wt% PBMA is 4.2 V vs. Li⁺/Li, showing good electrochemical

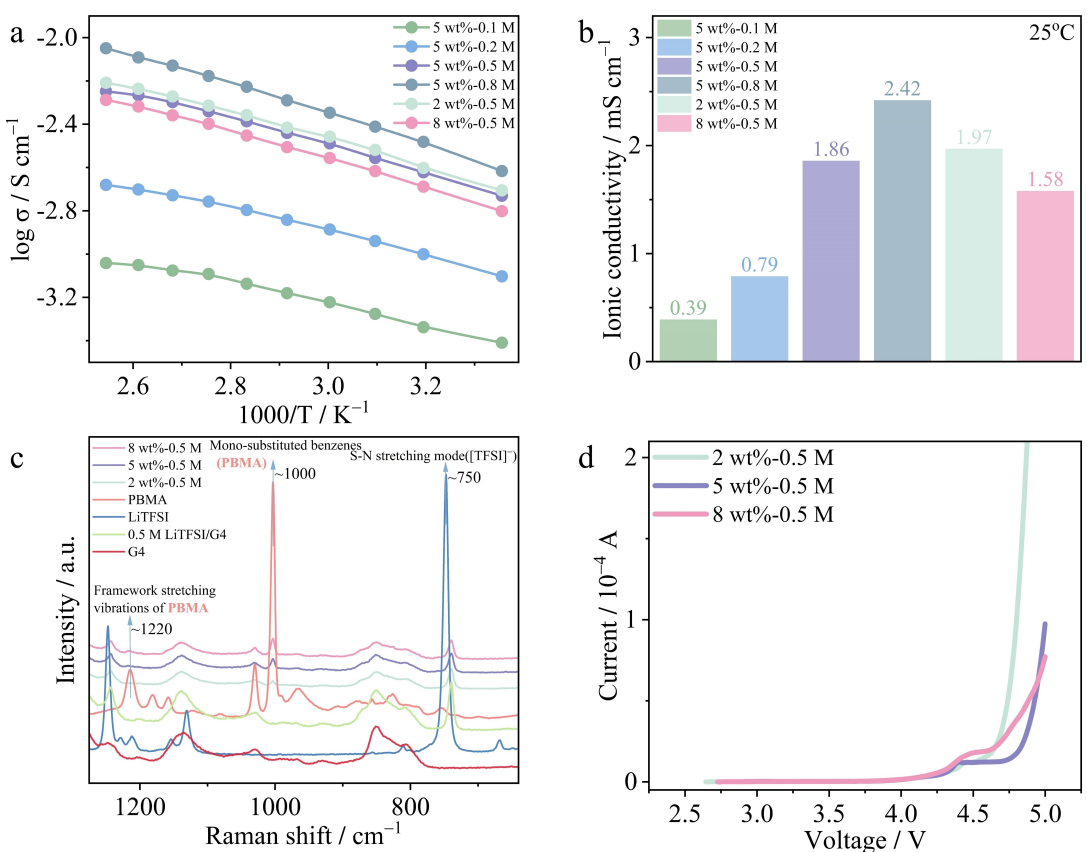


Figure 1. Characterization of PBMA-LiTFSI/G4 electrolytes. (a) Temperature dependence of ionic conductivity. (b) Ionic conductivity at 25 °C. (c) Raman analysis. (d) Linear sweep voltammetry test of PBMA-0.5 M LiTFSI/G4 electrolytes at 25 °C, with a scan rate of 0.1 mV s⁻¹.

oxidative stability. Furthermore, compared with 2 and 8 wt%, the battery with 5 wt% PBMA electrolytes also has the best cycling performance (see Figure 2b.). Consequently, the concentration of PBMA is selected to be 5 wt%. In conclusion, the optimal concentration is preliminarily determined to be 5 wt% PBMA-0.5 M LiTFSI/G4.

Subsequently, Li | LiFePO₄ cells are assembled with different PBMA-LiTFSI/G4 electrolytes and the carbonate-based electrolyte (1 M LiPF₆/EC-EMC (3:7, v/v)). Figure 2a shows the charge-discharge curves of the cells with different electrolytes at the first cycle. The charging voltage platform of the PBMA-LiTFSI/G4 electrolyte is ~11 mV higher than that of the carbonate-based electrolyte (see Figure S1), showing a slight polarization. The comparison of cycling performance of cells with various electrolytes (0.25 C) at 25 °C is depicted in Figure 2b. In the first ten cycles, the discharge capacity of cells is increasing steadily because of the activation process. Therefore, we take the tenth cycle capacity as the benchmark. Next, we analyze the impact of LiTFSI concentration (where PBMA is 5 wt%) on cell performance with PBMA-LiTFSI/G4 system. The cell with 0.2 M LiTFSI delivers a low-capacity retention of 79.46% and low average discharge capacity of 138.89 mAh g⁻¹ after 200 cycles. This behavior may be attributed to the low ion conductivity of the 0.2 M LiTFSI electrolyte, which hinders the smooth and rapid migration of Li⁺, ultimately affecting the cycle performance of the cell. The capacity retention of cells is

93.50 and 93.97% for the 0.5 and 0.8 M LiTFSI, respectively. The cells with 0.5 and 0.8 M LiTFSI exhibit an average discharge capacity of 149.88 and 147.93 mAh g⁻¹, and average Coulombic efficiency of 99.86 and 99.74%, respectively. The cells with 0.5 and 0.8 M LiTFSI demonstrate similar capacity retention, but the average discharge capacity and average Coulombic efficiency of 0.5 M LiTFSI are slightly better than those of 0.8 M LiTFSI. Compared to 0.8 M LiTFSI, 0.5 M LiTFSI has superior long-term cycling performance. Therefore, we chose 0.5 M LiTFSI as the optimal concentration.

In the next step, we discuss the influence of PBMA concentration (where the concentration of LiTFSI is 0.5 M) on cycling performance of cells with PBMA-LiTFSI/G4 system (Figure 2b). The capacity retention of the cells is 90.74, 93.50 and 88.27% for the 2, 5 and 8 wt% PBMA, respectively. The cells with 2, 5 and 8 wt% PBMA deliver an average discharge capacity of 144.99, 149.88 and 146.33 mAh g⁻¹. The data shows that the cell with 5 wt% PBMA exhibits high discharge capacity and excellent long-term cycling stability. This is probably caused by two reasons: Firstly, the previous Raman analysis demonstrates that there is an interaction between PBMA and LiTFSI, which makes the cycling performance of cell with 5 wt% PBMA better than that of 2 wt% PBMA. Secondly, excessive PBMA may lead to an increase in system viscosity, resulting in the cycling performance of cell with 5 wt% PBMA better than

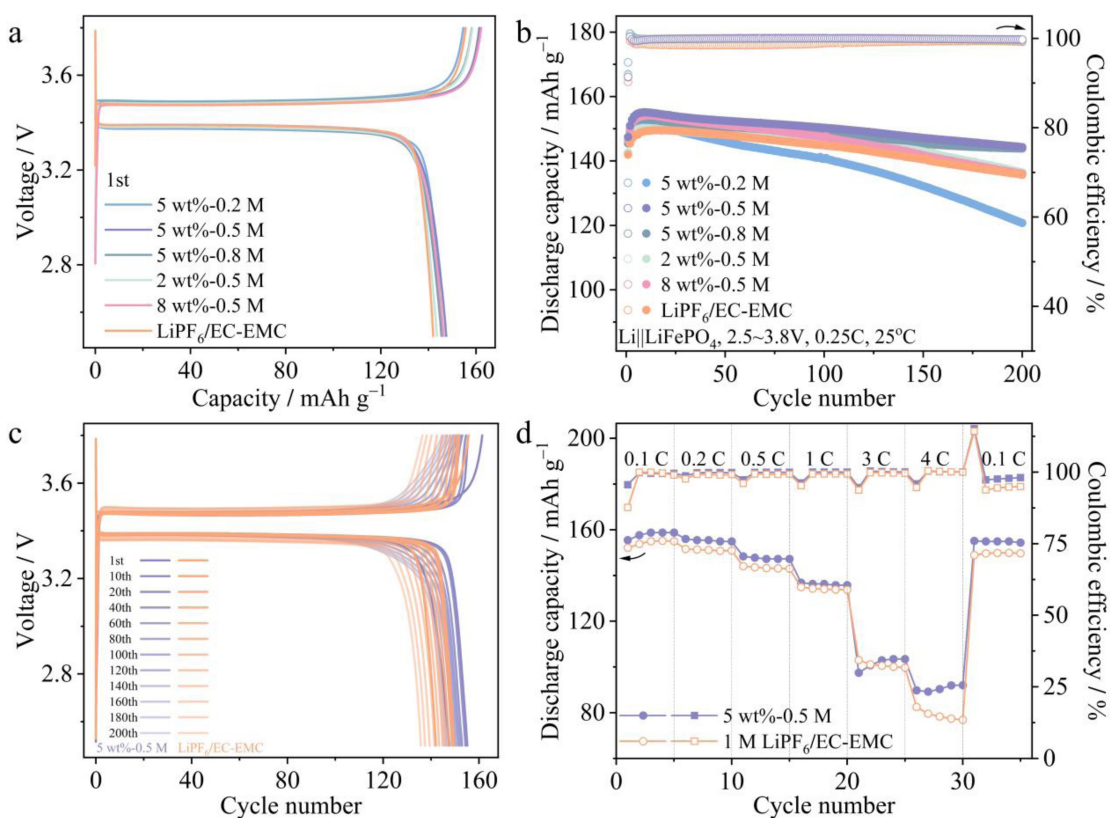


Figure 2. Li||LiFePO₄ batteries using both PBMA-LiTFSI/G4 electrolytes and the carbonate-based electrolyte. (a) Charge-discharge curves at the first cycle. (b) Cycling performance at 25 °C and 0.25 C rate. (c) Charge/discharge curves for 200 cycles. (d) Rate capability.

that of 8 wt% PBMA. Based on these results, the optimal combination is 5 wt% PBMA-0.5 M LiTFSI/G4.

Moreover, compared to 5 wt% PBMA-0.5 M LiTFSI/G4 (5 wt%-0.5 M), the cell with 1 M LiPF₆/EC-EMC (LiPF₆/EC-EMC) demonstrates slightly lower discharge capacity of 143.98 mAh g⁻¹, lower capacity retention of 90.85% and lower average Coulombic efficiency of 98.91% after 200 cycles (Figure 2b). As shown in Figure 2c, the cell with LiPF₆/EC-EMC exhibits similar charge-discharge curves with 5 wt%-0.5 M, but LiPF₆/EC-EMC shows larger polarization after 200 cycles. This is because for the carbonate-based electrolyte is difficult to form the stable solid-electrolyte interphase (SEI) on the surface of the lithium metal anode, which shows poor compatibility with the lithium negative electrode, resulting in a poor battery performance.^[46-49] In addition, 5 wt%-0.5 M endows an excellent rate capability, and the cell can achieve a discharge capacity of 157.86, 155.33, 147.57, 136.18, 101.59 and 90.65 mAh g⁻¹ at rates of 0.1, 0.2, 0.5, 1, 3 and even 4 C, respectively (Figure 2d). By contrast, the cell with LiPF₆/EC-EMC delivers a discharge capacity of 156.15, 153.87, 146.18, 137.06, 102.02 and 85.46 mAh g⁻¹ under the same conditions, respectively. Furthermore, the cell with 5 wt%-0.5 M exhibits a higher energy efficiency than that of LiPF₆/EC-EMC (Figure S3, Supporting Information). As shown in Figure S4, electrochemical stability against Li is evaluated using Li||Li symmetric cells. The cell with 5 wt%-0.5 M exhibits smooth and flat charge-discharge plateaus, while LiPF₆/EC-EMC generates unstable SEI

on the surface of Li, leading to voltage instability at the start of plating and at the end of stripping.

The resistance of LiFePO₄ batteries is investigated by electrochemical impedance spectroscopy (EIS) (Figure S5). The semicircle at high frequencies is designated to the interfacial charge transfer resistance on the electrode surface (R_{ct}), while the sloping line at low frequencies corresponds to Li⁺ diffusion into the LiFePO₄ phase.^[50,51] The R_{ct} of cells with LiPF₆/EC-EMC is higher than that with 5 wt%-0.5 M after 200 cycles, indicating 5 wt%-0.5 M shows better cycling stability. The morphology of LiFePO₄ cathode is observed via scanning electron microscopy (SEM) (Figure S6). We find that the formation of a large number of random big cracks on the LiFePO₄ cathode with LiPF₆/EC-EMC. These big cracks cause a poor cycling stability and Coulombic efficiency of the cell with LiPF₆/EC-EMC.^[52-54]

2.2. Characterization of the Thermal Protection and Reversibility of the Electrolyte

Next, we study the discharge performance of Li||LiFePO₄ batteries at various temperatures. Figure 3a-3b shows the performance of the cell with the LiPF₆/EC-EMC electrolyte from 25 to 105 °C. The cell shows an average discharge capacity of 147.06 mAh g⁻¹ at 25 °C. When the temperature rises from 65 to 95 °C, the discharge voltage platform of the battery has no obvious changes, which may be due to the fast ion transfer rate

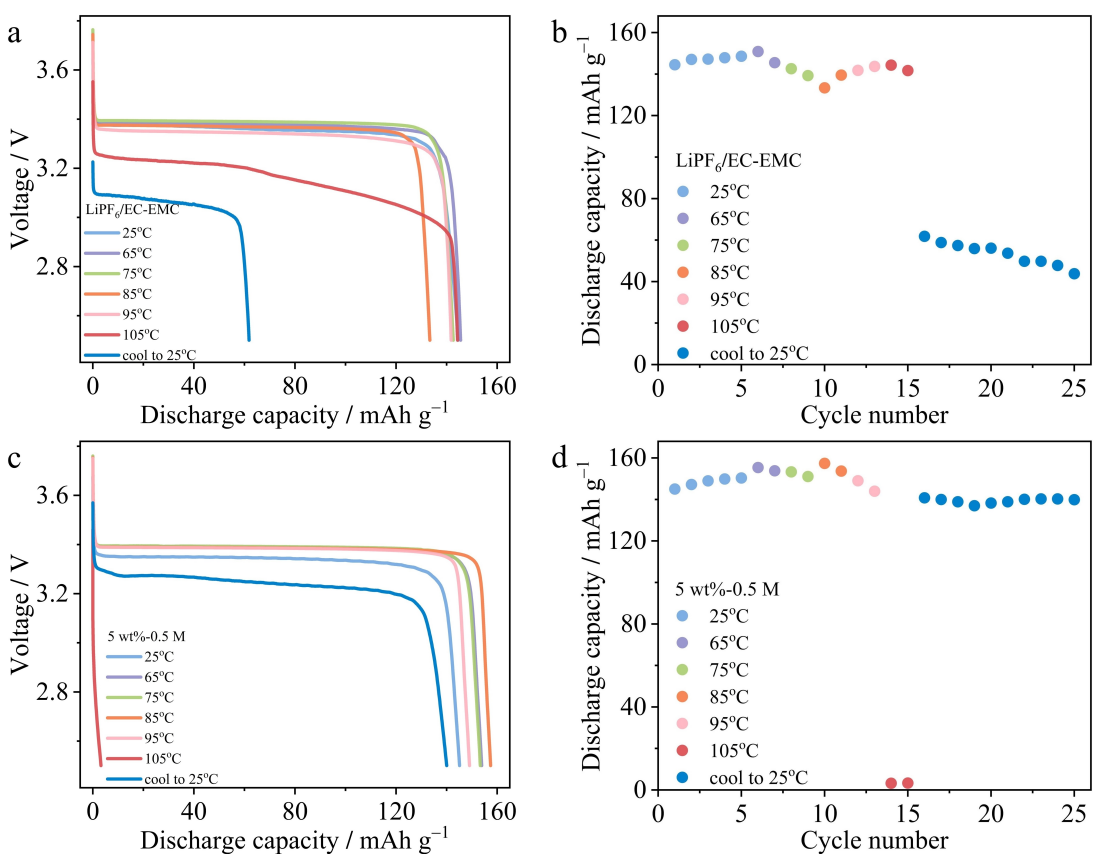


Figure 3. Relationship of between the discharge performance of $\text{Li} \parallel \text{LiFePO}_4$ batteries and temperature increase from 25 to 105 °C, then cool down to 25 °C. (a) Discharge curve and (b) discharge capacity of the cell assembled with 1 M LiPF_6 -EC/EMC. (c) Discharge curve and (d) discharge capacity of the cell assembled with 5 wt% PBMA-0.5 M LiTFSI/G4.

at high temperatures. Noted that the cells deliver an average discharge capacity of 148.20 and 142.75 mAh g⁻¹ at 65 and 95 °C, respectively. When the temperature further rises to 105 °C, the cell still shows an average discharge capacity of 143.0 mAh g⁻¹. In addition, when the temperature returns back to 25 °C, the cell exhibits a low-capacity retention of 70.87% and low average discharge capacity of 53.49 mAh g⁻¹ after 10 cycles. These data show that the $\text{Li} \parallel \text{LiFePO}_4$ battery with the LiPF_6 /EC-EMC electrolyte has high discharge capacity at high temperatures, while the cycle stability of the battery is poor when the temperature returns to 25 °C. By contrast, cells with the 5 wt%-0.5 M electrolyte deliver an average discharge capacity of 148.29 at 25 °C, as shown in Figure 3c-d. The discharge voltage plateau shows an upward trend and the average discharge capacity within 152.21~155.56 mAh g⁻¹ when the temperature is increased from 65 to 85 °C. When the temperature further increases to 95 °C, the discharge voltage plateau slightly decreases and the corresponding average discharge capacity is 146.51 mAh g⁻¹. However, when the temperature reaches to 105 °C, the discharge voltage of the cell sharply drops to the cut-off voltage of 2.5 V and the reversible capacity is only 3.23 mAh g⁻¹, showing a thermal shutdown phenomenon. Importantly, when the temperature returns back to 25 °C, the cell exhibits an excellent capacity retention of 99.36%, a high discharge capacity of 139.45 mAh g⁻¹ and the

capacity of the battery resumes 94% of the initial capacity at 25 °C after 10 cycles. These results show that the 5 wt%-0.5 M electrolyte has the characteristics of combining a thermal response and a shutdown at 105 °C, which can provide highly accurate and reversible thermal protection for batteries. We hypothesize that this phenomenon is associated with the phase separation of the electrolyte, which will be further validated by the data from differential scanning calorimeter (DSC), EIS, and SEM tests (Figure 4 and S8).

In order to explain this phenomenon about the thermal cut-down behavior of the $\text{Li} \parallel \text{LiFePO}_4$ battery at high temperatures, we test the DSC of the 5 wt%-0.5 M electrolyte, as shown in Figure 4a. The electrolyte mass retention is 98.02% at 120 °C, showing a good thermal stability (see Figure S9). The DSC curve exhibits an endothermic peak at 93 °C, which is ascribed to the LCST phase separation behavior of the electrolyte. This conclusion is consistent with the previous literature,^[55] being 93 °C the LCST of the electrolyte. However, the phase separation process is not instantly completed. The phase separation behavior of a system composed of PBMA and 1-butyl-3-methylimidazolium bis(trifluoromethanesulfonyl) imide ([BMIM][TFSI]) has been studied and the LCST of 2 wt% PBMA/[BMIM][TFSI] solution is 136.5 °C.^[56] The phase separation of this solution begins at 136.5 °C and separates into two phases completely at 152 °C. This study indicates that the homoge-

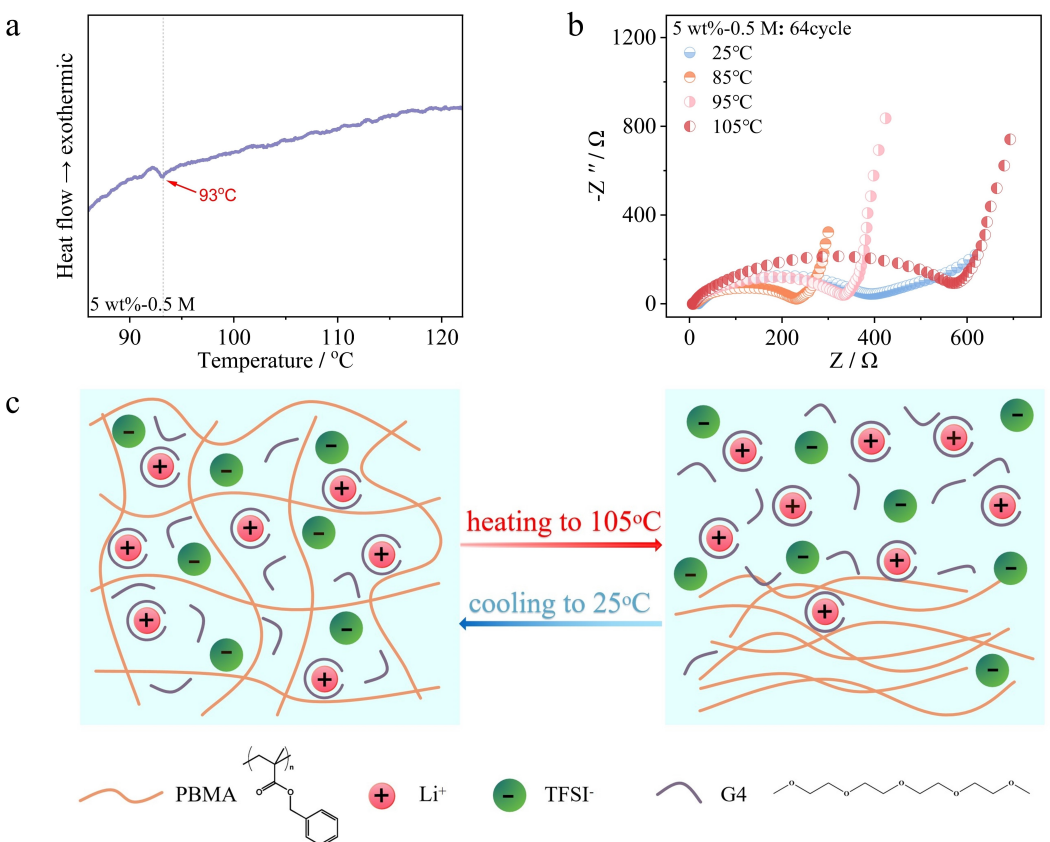


Figure 4. (a) DSC curves of the 5 wt % PBMA-0.5 M LiTFSI/G4 electrolyte at a ramp rate of $2^{\circ}\text{C min}^{-1}$. (b) EIS results of the $\text{Li} \parallel \text{LiFePO}_4$ battery cycled after 64 cycles, then placed at different temperatures for 10 min. (c) Schematic diagram of the 5 wt % PBMA-0.5 M LiTFSI/G4 electrolyte at 25 and 105 °C.

neous solution completely separates into two phases at $>$ LCST. Similarly, the LCST of the 5 wt%–0.5 M electrolyte through DSC results is 93 °C, which means that phase separation of the electrolyte starts at 93 °C. As the temperature further increases, the homogeneous phase of the electrolyte separates into a low conductivity PBMA-rich phase and a high conductivity phase with G4 and LiTFSI. Therefore, when the temperature is below LCST, the electrolyte is homogeneous and the cell performance is only affected by temperature (Figure 4c). The ion transfer rate is faster as the temperature rises, resulting in an increase in battery performance (Figure 3c–d). When the temperature exceeds the LCST, the electrolyte begins to exhibit a phase separation behavior. Thus, the cell performance is influenced by the temperature and by the electrolyte state. The temperature 95 °C is close to the LCST and the electrolyte is not yet completely separated into two phases. So, the discharge capacity of the cell at 95 °C is slightly lower than that at 85 °C. When the temperature reaches 105 °C, the discharge voltage of the cell drops rapidly, and the discharge capacity is less than 4 mAh g⁻¹. The results show that the phase separation of the electrolyte is basically completed at 105 °C (Figure 4c). The PBMA-rich phase is deposited on the electrode surface that can block the Li⁺ insertion reactions effectively and switch off battery operation, as displayed in Figure 4c. Therefore, the electrolyte provides a thermal protection for the battery at 105 °C. When the temperature returns back to 25 °C, the

5 wt%–0.5 M electrolyte resumes as a homogeneous phase. The possible shut-down mechanism is shown in Figure 4c. Importantly, the capacity of the battery resumes at 94% after 10 cycles (Figure 3d). Consequently, the 5 wt%–0.5 M electrolyte can provide highly accurate and reversible, thermoswitchable self-protection for the battery.

To further verify this behavior, EIS is used to explore the resistance of cell with the 5 wt%–0.5 M electrolyte at different temperatures (Figure 4b). The R_{ct} of the cell at 25, 85, 95 and 105 °C is 339.2, 230.1, 335.5 and 623.8 Ω, respectively, which indicates that the R_{ct} increases and then decreases as the temperature increases. Below the LCST, the ion transfer rate becomes faster, resulting in a decrease in R_{ct}. Furthermore, above the LCST, the electrolyte separates into two phases, resulting in an increase in R_{ct}. Finally, SEM is used to observe the surface morphology of the cell. As shown in Figure S8, the microstructure of LiFePO₄ cathode does not show obvious change before and after high-temperature testing. This observation indicates that the 5 wt%–0.5 M electrolyte does not undergo severe side reactions with the cathode at high temperatures, and the cathode microstructure is not destroyed, providing a strong guarantee for the recovery of battery performance after high temperatures.

Since we cannot directly observe the color change of the electrolyte, we test the voltage-time curve of the battery with this electrolyte at 105 °C and then cooling down to 25 °C. The

results are shown in Figure 5a. The voltage decreases to 3.4 V suddenly, and then the cell nearly cannot be discharged. After cooling down to 25 °C for 5 h, the cell recovers its normal charge/discharge voltage curves and capacity. Furthermore, the effect of high-temperature storage of the LiFePO₄ battery with the 5 wt%–0.5 M electrolyte at 105 °C is investigated (Figure 5b). At 25 °C, the cell delivers an average discharge capacity of 153.05 mAh g⁻¹ after 60 cycles and discharge capacity of 151.64 mAh g⁻¹ at the 60th cycle. After experiencing 105 °C thermal abuse for 5 hours, the cell exhibits a discharge capacity of 145.29 mAh g⁻¹ at the first cycle. Moreover, the discharge capacity of the cell slowly decreases with an average discharge capacity of 135.92 mAh g⁻¹, average Coulombic efficiency as high as 95.52%, and capacity retention of 85.17% after 100 cycles. This good high-temperature recovery performance should be attributed to the excellent thermal reversibility of the electrolyte.

Finally, the application of cells at a temperature of 60 °C is also explored. As shown in Figure 5c, the discharge capacity and Coulombic efficiency of the cell with LiPF₆/EC-EMC electrolyte greatly decline, and the discharge capacity decreases from 140.5 to 103.8 mAh g⁻¹ in the first 17 cycles and then the reversible capacity sharply decreases to 0 mAh g⁻¹. In contrast, the battery with the 5 wt%–0.5 M electrolyte exhibits good temperature cycling performance with an average discharge capacity of 152.48 mAh g⁻¹ at 60 °C, average Coulombic effi-

ciency of 98.84%, and capacity retention of 95.6% in the first 17 cycles. Moreover, the cell with 140.53 mAh g⁻¹ average discharge capacity and 97.78% average Coulombic efficiency is obtained after 100 cycles at 60 °C. These results indicate that cells with the 5 wt%–0.5 M electrolyte exhibit a good 60 °C high-temperature cycle stability.

3. Conclusions

In summary, this study introduces a temperature-responsive, self-protection electrolyte comprising 5 wt% PBMA, 0.5 M LiTFSI, and G4, imbuing Li||LiFePO₄ batteries with temperature-aware, responsive, and recovery capabilities. Through the phase separation phenomenon inherent in this electrolyte, high temperatures (105 °C) trigger the segregation of the electrolyte into a low conductivity PBMA-rich phase and a high conductivity phase containing LiTFSI/G4. This deposition of the PBMA-rich phase onto the electrode surface effectively inhibits ion transport, abruptly halting battery operation. Upon returning to room temperature, the electrolyte reverts to a homogeneous, highly conductive phase, enabling the battery to resume approximately 94% of its capacity after 10 cycles. Hence, the 5 wt%–0.5 M electrolyte offers highly precise and reversible thermoswitchable self-protection for batteries. Furthermore, this electrolyte demonstrates exceptional room-temperature

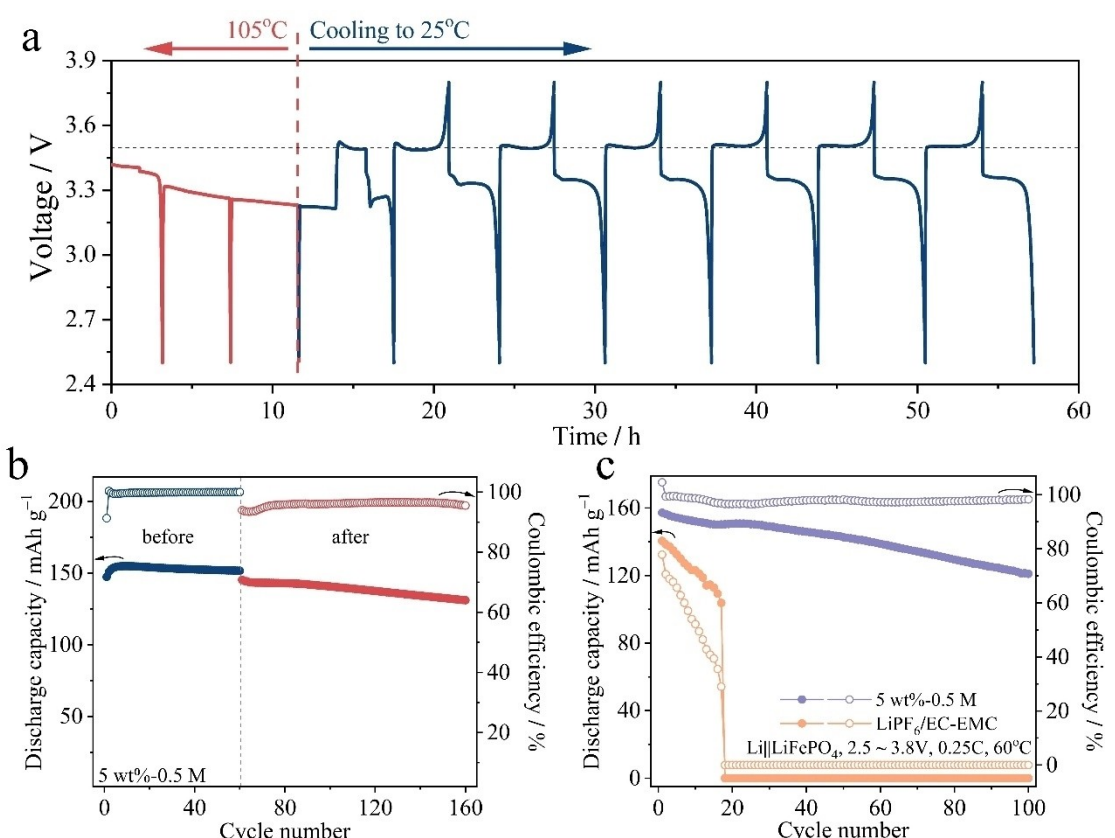


Figure 5. (a) Voltage-time curve of the battery with this 5 wt% PBMA-0.5 M LiTFSI/G4 electrolyte at 105 °C and then cooling down to 25 °C. (b) Cycling performance of Li||LiFePO₄ battery using 5 wt% PBMA-0.5 M LiTFSI/G4 electrolyte at 25 °C before and after storage at 105 °C for 5 hours. (c) The cycling performance of Li||LiFePO₄ batteries using 5 wt% PBMA-0.5 M LiTFSI/G4 and 1 M LiPF₆-EC/EMC electrolyte at 60 °C.

cycling performance and robust high-temperature shutdown characteristics. Our research yields fresh insights and perspectives into thermo-reversible and self-protective electrolytes, thereby facilitating the safe and widespread adoption of lithium-ion batteries.

4. Supporting Information

Supporting Information is available from the Wiley Online Library or from the author.

Acknowledgements

This work is financially supported by the National Natural Science Foundation of China (no. 22075155), the Zhejiang Provincial Natural Science Foundation of China Grant (Grant No. LY24B030002), and the Ningbo Science & Technology Innovation 2025 Major Project (no. 2021Z121). Peter Müller-Buschbaum acknowledges the financial support from Deutsche Forschungsgemeinschaft (DFG, German Research Foundation) under Germany's Excellence Strategy – EXC 2089/1 – 390776260 (e-conversion). Qian Yu and Wei Sun contributed equally to this work. Lan Xia acknowledges the China Scholarship Council (CSC) and the Ningbo Science and Technology Bureau (2024QL036). Open Access funding enabled and organized by Projekt DEAL.

Conflict of Interests

The authors declare no conflict of interest.

Data Availability Statement

The data that supports the findings of this study are available from the corresponding author upon reasonable request.

Keywords: lithium-ion batteries • safety protection • thermal runaway • phase separation • poly (butyl methacrylate)

- [1] F. X. Wu, J. Maier, Y. Yu, *Chem. Soc. Rev.* **2020**, *49*(5), 1569–1614.
- [2] Z. M. Tong, J. Z. Miao, J. L. Mao, Z. Y. Wang, Y. Y. Lu, *Energy Storage Mater.* **2022**, *50*, 533–542.
- [3] Q. S. Wang, B. B. Mao, S. I. Stoliarov, J. H. Sun, *Prog. Energy Combust. Sci.* **2019**, *73*, 95–131.
- [4] K. Xu, *Chem. Rev.* **2014**, *114*(23), 11503–11618.
- [5] M. Z. Liu, J. Vatamanu, X. L. Chen, L. D. Xing, K. Xu, W. S. Li, *ACS Energy Lett.* **2021**, *6*(6), 2096–2102.
- [6] A. M. Haregewoin, A. S. Wotango, B. J. Hwang, *Energy Environ. Sci.* **2016**, *9*(6), 1955–1988.
- [7] H. Jia, B. Billmann, H. Onishi, J. Smiatek, S. Roeser, S. Wiemers-Meyer, R. Wagner, M. Winter, I. Cekic-Laskovic, *Chem. Mater.* **2019**, *31*(11), 4025–4033.
- [8] J. G. Han, K. Kim, Y. Lee, N. S. Choi, *Adv. Mater.* **2019**, *31*(20), 1804822.
- [9] G. Mandouma, J. Collins, D. Williams, *Acc. Chem. Res.* **2023**, *56*(11), 1263–1270.
- [10] K. Kim, D. Hwang, S. Kim, S. O. Park, H. Cha, Y. S. Lee, J. Cho, S. K. Kwak, N. S. Choi, *Adv. Energy Mater.* **2020**, *10*(15), 2000012.
- [11] L. Chen, X. H. Shen, H. Chen, T. Z. Wen, R. H. Rao, C. L. Zhang, Q. F. Meng, J. Zhang, Y. Ding, X. P. Ai, Y. L. Cao, Z. X. Chen, *Energy Storage Mater.* **2023**, *55*, 836–846.
- [12] Y. Yamada, J. H. Wang, S. Ko, E. Watanabe, A. Yamada, *Nat. Energy* **2019**, *4*(4), 269–280.
- [13] Z. Geng, J. Z. Lu, Q. Li, J. L. Qiu, Y. Wang, J. Y. Peng, J. Huang, W. J. Li, X. Q. Yu, H. Li, *Energy Storage Mater.* **2019**, *23*, 646–652.
- [14] S. Y. Yuan, K. Ding, X. Y. Zeng, D. Bin, Y. J. Zhang, P. Dong, Y. G. Wang, *Adv. Mater.* **2023**, *35*(13), 2206228.
- [15] X. Y. Chen, S. S. Yan, T. H. Tan, P. Zhou, J. X. Hou, X. N. Feng, H. Dong, P. C. Wang, D. Wang, B. G. Wang, M. G. Ouyang, K. Liu, *Energy Storage Mater.* **2022**, *45*, 182–190.
- [16] X. N. Feng, D. S. Ren, X. M. He, M. G. Ouyang, *Joule* **2020**, *4*(4), 743–770.
- [17] D. Lu, S. H. Zhang, J. D. Li, L. Huang, X. H. Zhang, B. Xie, X. C. Zhuang, Z. L. Cui, X. L. Fan, G. J. Xu, X. F. Du, G. L. Cui, *Adv. Energy Mater.* **2023**, *13*(28), 2300684.
- [18] L. C. Kong, Y. Li, W. Feng, *Electrochem. Energy Rev.* **2021**, *4*(4), 633–679.
- [19] X. N. Feng, M. G. Ouyang, X. Liu, L. G. Lu, Y. Xia, X. M. He, *Energy Storage Mater.* **2018**, *10*, 246–267.
- [20] Y. Y. Xiao, M. Y. Yan, L. Shi, L. I. Gong, X. D. Cheng, H. P. Zhang, Y. L. Pan, *Energy Storage Mater.* **2023**, *61*, 102871.
- [21] L. Li, C. Jia, Y. Liu, B. Fang, W. Q. Zhu, X. Y. Li, L.-A. Schaefer, Z. W. Li, F. S. Zhang, X. N. Feng, N. Hussain, X. Q. Xi, D. Wang, Y.-H. Lin, X. D. Wei, H. Wu, *Mater. Today* **2022**, *54*, 72–82.
- [22] W. X. Ji, F. Wang, D. T. Liu, J. F. Qian, Y. L. Cao, Z. X. Chen, H. X. Yang, X. P. Ai, *J. Mater. Chem. A* **2016**, *4*(29), 11239–11246.
- [23] H. Li, F. Wang, C. R. Zhang, W. X. Ji, J. F. Qian, Y. L. Cao, H. X. Yang, X. P. Ai, *Energy Storage Mater.* **2019**, *17*, 275–283.
- [24] K. Liu, W. Liu, Y. C. Qiu, B. A. Kong, Y. M. Sun, Z. Chen, D. Zhuo, D. C. Lin, Y. Cui, *Sci. Adv.* **2017**, *3*(1), e1601978.
- [25] F. N. Jiang, X. B. Cheng, S. J. Yang, J. Xie, H. Yuan, L. Liu, J. Q. Huang, Q. Zhang, *Adv. Mater.* **2023**, *35*(12), 2209114.
- [26] J. N. Zhang, H. Wu, X. F. Du, H. Zhang, L. Huang, F. Sun, T. T. Liu, S. W. Tian, L. X. Zhou, S. J. Hu, Z. X. Yuan, B. T. Zhang, J. J. Zhang, G. L. Cui, *Adv. Energy Mater.* **2022**, *13*(3), 2202529.
- [27] L. Xia, S. L. Li, X. P. Ai, H. X. Yang, Y. L. Cao, *Energy Environ. Sci.* **2011**, *4*(8), 2845–2848.
- [28] W. X. Ji, B. L. Jiang, F. X. Ai, H. X. Yang, X. P. Ai, *RSC Adv.* **2015**, *5*(1), 172–176.
- [29] Z. Z. Liu, Q. Yu, N. Oli, J. F. F. Gomez, S. Qiu, H. R. Tian, Q. Qiu, W. Sun, K. H. Li, Z. S. Liu, M. M. Chen, J. L. Yuan, X. Y. Wu, L. Xia, *Adv. Energy Mater.* **2023**, *13*(22), 2300143.
- [30] J. C. Kelly, R. Gupta, M. E. Roberts, *J. Mater. Chem. A* **2015**, *3*(7), 4026–4034.
- [31] J. C. Kelly, N. L. Degroot, M. E. Roberts, *Chem. Commun.* **2015**, *51*(25), 5448–5451.
- [32] B. R. Carrick, C. L. Seitzinger, T. P. Lodge, *Molecules* **2021**, *26*(16), 4850.
- [33] Q. L. Zhang, C. Weber, U. S. Schubert, R. Hoogenboom, *Mater. Horiz.* **2017**, *4*(2), 109–116.
- [34] Q. Zhang, S. Y. Dong, M. M. Zhang, F. H. Huang, *Aggregate* **2021**, *2*(1), 35–47.
- [35] X. Y. Ma, J. T. Yu, Y. Hu, J. Texter, F. Yan, *Ind. Chem. Mater.* **2023**, *1*(1), 39–59.
- [36] Y. Kobayashi, Y. Kitazawa, K. Hashimoto, T. Ueki, H. Kokubo, M. Watanabe, *Langmuir* **2017**, *33*(49), 14105–14114.
- [37] S. M. Zhang, G. J. Yang, Z. P. Liu, X. Y. Li, X. F. Wang, R. J. Chen, F. Wu, Z. X. Wang, L. Q. Chen, *Nano Lett.* **2021**, *21*(7), 3310–3317.
- [38] L. P. Hou, X. Q. Zhang, B. Q. Li, Q. Zhang, *Angew. Chem. Int. Ed.* **2020**, *59*(35), 15109–15113.
- [39] L. Chen, J. H. Lu, Y. B. Wang, P. He, S. B. Huang, Y. Liu, Y. Z. Wu, G. P. Cao, L. Wang, X. M. He, J. Y. Qiu, H. Zhang, *Energy Storage Mater.* **2022**, *49*, 493–501.
- [40] C. F. He, J. Q. Liu, J. Li, F. F. Zhu, H. J. Zhao, *J. Membr. Sci.* **2018**, *560*, 30–37.
- [41] J. Q. Cui, J. Q. Liu, C. F. He, J. Li, X. F. Wu, *J. Membr. Sci.* **2017**, *541*, 661–667.
- [42] J. Q. Liu, X. F. Wu, J. Y. He, J. Li, Y. Q. Lai, *Electrochim. Acta* **2017**, *235*, 500–507.
- [43] A. L. Phan, C. Jayawardana, P. M. L. Le, J. X. Zhang, B. Nan, W. R. Zhang, B. L. Lucht, S. Y. Hou, C. S. Wang, *Adv. Funct. Mater.* **2023**, *33*(34), 2301177.

- [44] Y. B. Xiao, X. F. Wang, K. Yang, J. Y. Wu, Y. Chao, C. P. Xi, M. C. Li, Q. L. Zhang, Z. Y. Liu, L. Y. Li, Y. Yu, C. K. Yang, *Energy Storage Mater.* **2023**, *55*, 773–781.
- [45] J. Ming, Z. Cao, W. Wahyudi, M. L. Li, P. Kumar, Y. Q. Wu, J. Y. Hwang, M. N. Hedhili, L. Cavallo, Y. K. Sun, L. J. Li, *ACS Energy Lett.* **2018**, *3*(2), 335–340.
- [46] W. Q. Fang, Z. X. Wen, L. Chen, Z. Y. Qin, J. Q. Li, Z. C. Zheng, Z. Weng, G. Wu, N. Zhang, X. H. Liu, X. M. Yuan, G. Chen, *Nano Energy* **2022**, *104*, 107881.
- [47] J. Y. Wu, Z. X. Rao, X. T. Liu, Y. Shen, C. Fang, L. X. Yuan, Z. Li, W. X. Zhang, X. L. Xie, Y. H. Huang, *Adv. Mater.* **2021**, *33*(12), 2007428.
- [48] Y. Z. Zhu, X. Li, Y. B. Si, X. Q. Zhang, P. F. Sang, Y. Z. Fu, *J. Energy Chem.* **2022**, *73*, 422–428.
- [49] J. B. Zhang, H. K. Zhang, S. T. Weng, R. H. Li, D. Lu, T. Deng, S. Q. Zhang, L. Lv, J. C. Qi, X. Z. Xiao, L. W. Fan, S. J. Geng, F. H. Wang, L. X. Chen, M. Noked, X. F. Wang, X. L. Fan, *Nat. Commun.* **2023**, *14*(1), 2211.
- [50] Y. B. Xu, H. P. Wu, Y. He, Q. S. Chen, J. G. Zhang, W. Xu, C. M. Wang, *Nano Lett.* **2020**, *20*(1), 418–425.
- [51] C. Peng, J. Jin, G. Z. Chen, *Electrochim. Acta* **2007**, *53*(2), 525–537.
- [52] M. Yeddala, L. Rynearson, B. L. Lucht, *ACS Energy Lett.* **2021**, *8*(11), 4782–4793.
- [53] J. G. Kim, D. Gu, K. H. Cho, C. Y. Im, S. J. Kim, *Small* **2023**, *19*(37), 2301207.
- [54] S. R. Chen, J. M. Zheng, D. H. Mei, K. S. Han, M. H. Engelhard, W. G. Zhao, W. Xu, J. Liu, J. G. Zhang, *Adv. Mater.* **2018**, *30*(21), 1706102.
- [55] K. Fujii, T. Ueki, K. Niitsuma, T. Matsunaga, M. Watanabe, M. Shibayama, *Polymer* **2011**, *52*(7), 1589–1595.
- [56] H. N. Lee, T. P. Lodge, *J. Phys. Chem. B* **2011**, *115*(9), 1971–1977.

Manuscript received: May 24, 2024
Revised manuscript received: June 18, 2024
Accepted manuscript online: June 19, 2024
Version of record online: August 2, 2024